*REVISED Manuscript (Clean version)
Click here to view linked References

Licencia Creative Commons CC BY-NC-ND

Environmental risks and mechanical evaluation of recycling red mud in bricks

F. Arroyo, Y. Luna-Galiano, C. Leiva*, L.F. Vilches, C. Fernández-Pereira

Higher Technical School of Engineering. Chemical and Environmental Engineering Department. University of Seville, Spain. Phone: +34 954487269; FAX: +34 954461775; e-mail: cleiva@us.es

Abstract

More and more by-products are being used in several materials, especially in construction industry. Natural construction materials contain amounts of heavy metals and radionuclides, but when by-products are used in this kind of materials, this could generate to a growth of their concentrations and have an impact on public health.

In this paper, red mud was used as a raw material (as clay substitute) to fabricate fired bricks. Physical, mechanical, radiological and heavy metals leaching properties of fired bricks with a replacement ratio of up to 80%wt of clay by red mud were discussed. Indeed, the effect of different sintering temperatures (1173 and 1373K) was analyzed, and results show that the higher the temperature produces the higher the mechanical strength.

To environmentally characterize materials, they were subjected to two different leaching tests, a batch test for raw materials and a monolithic test for the bricks. The results obtained were compared with the limits stated for several heavy metals by the European Landfill Directive. Results showed that red mud gives leachate concentration values for Cr higher than the limits stated for non-hazardous by-products. Bricks do not show the same problem, although in the case of V a high concentration is observed, in the samples containing a high RM proportion and fabricated at low sintering temperature (1173K).

The contents of radionuclides such as 220 Ra, 232 Th and 40 K of the final construction materials were analyzed and compared with different indexes.

This paper has stated the maximum amounts of RM that can be used to replace clay for the manufacture of fired bricks without environmental risk.

Author Keywords: fired brick; red mud; clay; compressive strength; heavy metals leaching, natural radionuclides.

1. Introduction

Bricks are commonly used in construction since their discovery in 7500 BC. At present, fired bricks are mainly made with clay at high temperature firing (Zhang 2013). Clay production processes are energy intensive and produce high quantities of wastes and greenhouse gases (2.0 kWh and 0.41 kg of carbon dioxide per brick) (Zhang 2013). Many researches have been conducted related to the utilization of wide variety of by-product materials to substitute clay in the bricks production (Zhang 2013; Eliche-Quesada & Leite Costa, 2016; 2018; Maza-Ignacio et al, 2020, Luo et al, 2020; Rehman et al, 2020;; .

Red mud (RM) is a hazardous residue generated in the alumina production (Liu et al 2017). The worldwide production of RM was estimated about four billion tons, increasing at 150 million tons per year. This clearly necessitates the development and implementation of the reuse of large volumes of RM. But the safe recycling of this huge amount of alkaline waste is considered as serious challenges to the alumina industries due to its high alkalinity and contents of trace radioactive and heavy metals elements and it should be addressed in the different studies on RM`s recycling.

(He et al, 2011). Many researchers have studied different valorization routes of RM. Most promising options are the use as construction material, remediation of contaminated soils, the metals and rare earth elements recovery and other alternatives utilizing the alkalinity or the ion absorption capability (; Man et al 2017, Zhang et al, 2020; Mahinroosta et al, 2020; Oprckal et al, 2020; Wang et al, 2020)).

Using RM as secondary raw materials to produce bricks can realize comprehensive utilization of almost a 100% of the produced residue. Moreover, there were many substances in RM that can lower the sintering temperature to save energy and help form glassy phase to improve the strength of bricks. However, the factors causing problems during deposition (heavy metals, alkalinity, radioactivity, etc.) stay in RM. Therefore, the successful utilization of these kind of by-products (with enhanced concentrations) into bricks is conditioned by the demonstration that these materials do not involve a hazard to the environment nor health (He et al, 2011).

Construction Products Directive (European Commission, 2011) and specifically EN 771 (EN 771-1, 2016) for bricks, impose the obligation to not produce the construction materials influencing adversely human health and the environment. For example, EN 771 requires verification and declaration about the emission and sometimes the content of dangerous substances present in the bricks, but it does not stablish which substances should be studied, with what tests and what limits. RP-112 (European Commission, 1999) was the first comprehensive document issued by the European Commission, setting the principles of protection concerning the natural radioactivity, and stablishing two different dose criteria (1mSv /y and 0.3 mSv/y) for the maximum annual dose. Activity concentration index (ACI) was stablished as a tool to verify the maximum annual dose, calculated using the concentration of Th-232, Ra-226, and K-40 (see section 3.4). Later, the European Commission (European Commission, 2013) adopted the 1 mSv/y criteria (only Danish regulation requires 0.3 mSy/y (B192, 2002)). This index is also used in others regulations from different countries, but the coefficients for the ACI calculations are different, for example Israel (SI 5098, 2007).

From heavy metals point view, there is still no European legislation or recommendation that imposes a test and limits on the leaching of heavy metals in building materials. There are, however, several national (Italy (Italian Ministerial Decree 186, 2006) and Netherland (SQD, 2007)) and regional legislations (Catalonia (OVS, 1996) and the Basque Country (DPV, 2003) in Spain), but they use different test with different solid/water ratio, pH, samples (granular or monolith), time of exposure, and they stablish different limits although the leaching test even if they use the same test or they can only be applied to specific by-product.

In this paper, different RM dosages (0-50-80% of RM substitution) and sintering temperatures (1173K and 1373K) were studied. The temperatures were selected based on the RM sintering temperature and the typical temperature used in the industrial bricks fabrication, according to the previous literature (Pérez-Villarejo et al, 2012).

The effect of previous variables on the compressive strength, bulk density, shrinkage, mineral composition and microstructure of the final bricks were analyzed. The water absorption was also analyzed, as well as the leachate composition and radiological behavior in order to determine the impact of the RM recycling in bricks.

2. Raw Materials and Experimental Methods

2.1. Raw materials

Natural clay (CL) and Red mud (RM) from a Bayer process were used in this work.

2.2. Bricks production

Table 1 shows RM, CL and water weight compositions used in the production of bricks. Water content was varied with the RM content. Components were mixed for 4 minutes and wet pastes were deposited into cylindrical molds of 4 cm length and 3.3 cm diameter, and pressurized (5 MPa) during 5 minutes. Molding pressure is in the range than typical molding pressures (4-50 MPa) (Leiva et al, 2018). After that, samples were cured at 298K for 48 h, followed dried at 378K for 48 h more.

Table 1. Compositions of bricks (%wt)

2.3. Heating procedure

Two different heating cycles (Figure 1) were used for the fired of the bricks: 1) from 298K to 773K at 100K/h, 2) heating from 773K to the sintering temperature (1173 or 1373K) at 50K/h, and 3) maintaining the sintering temperature constant for 8h.

Figure 1. Heating program of bricks

2.4. Testing methods

2.4.1. Chemical, mineralogical and thermal characterization

Chemical compositions were determined by means of using X-Ray Fluorescence (Panalytical, AXIOS model). X-ray diffraction analysis (XRD) of RM, CL and bricks were carried out using a D8 Advance A25 (BRUKER) (40 kV and 30 mA) instrument; and DIFFRAC-EVA software (BRUKER) was used for phase identification. JCPS data has been PDF4.2019.

Mass changes with the temperature of the test specimens were determined using thermo-gravimetric analysis in duplicate. Tests were performed using a TA Instrument SDT Q600 analyzer using a heating rate of 20K/min in an air atmosphere (Leiva et al, 2016) from 293K to 1573K.

2.4.2. Mechanical and physical tests

Material bulk densities (ρ) were calculated through weight and volume of specimens according to EN 772-13 to four specimens of each type (EN772-13, 2013). The water absorption capacity was measured according to EN 772-21 in triplicate (EN 772-21, 2011). The compressive strength (Rc) (EN 772-1, 2016) was determined using a Tinius-Olsen TO 317 machine in triplicate.

2.4.3. Leaching test

When a material containing by-products is fired, on the one hand, there is a mass loss that increases the proportion of heavy metals; and on the other hand, the sintering process changes the matrix of the product and some heavy metals are stabilized. Since RM contains heavy metals, batch and monolithic leaching tests were also carried out to the raw materials and final bricks for a broader characterization.

EN 12457-4 (EN 12457-4, 2002) is a batch static extraction test with a liquid /solid ratio of 10 L/kg with 24 h of agitation. This test was carried out on the raw materials (red mud and clay). The second test is a monolithic test as defined in NEN 7375 (NEN 7375, 2005) and it was performed on the final bricks. According to the NEN 7375 test, fresh leaching solution (water at pH equal to7) must be changed 8 times. For this reason, this test is considered quite comparable to rain, the main leaching solution for exterior walls.

Metal content in leachates was analyzed using inductively coupled plasma-atomic emission spectroscopy. Both leaching tests were carried out in duplicate.

2.4.4. Radionuclide test

Bricks were reduced to a fine granulometry using a ball mill, introduced in a polystyrene Petri dish of 80 cm^3 volume, and later vacuum-sealed into a plastic bag in order to prevent 222-Rn scape, so that 226-Ra activity concentration can be determined through the gamma emission of 214-Pb. Activity concentration of 40-K was directly determined through its gamma emission of 1460 keV, while 232-Th activity concentration was derived through the gamma emissions from 228-Ac.

The principal gamma-ray detector was a low-background Canberra high-purity germanium (HPGe) GR-6022 reverse electrode coaxial detector with 60% relative efficiency, surrounded by a 10 cm thick high-purity lead shield. They were carried out in duplicate.

3. RESULTS

3.1 Characterization of RM and CL

Chemical compositions of RM and CL are shown in Table 2. RM contains a lower percentage of silica, mostly being non-reactive, than CL (75.66% wt), but the content of Al_2O_3 (18.08 % wt) in RM is higher than CL (11.25% wt). TiO_2 content of the RM is higher, while CL does not present a significant value. LOI value measures the volatile compounds that could be emitted during firing (due to chemical water bounded and the breakdown of calcite) and it is higher in RM than CL. Table 3 shows the minor components of RM which presents a considerable content of some heavy metals as Cr, Ba and V, and other components, as Th, which could be produced some radiological problems.

Table 2. Clay and red mud chemical characterization (%wt)

Table 3. Minor chemical components (ppm) of RM

The EN 12457-4 (EN 12457-4, 2002) leaching test was performed to RM to characterize the behavior of heavy metals leaching, In Italy, EN 12457-1 is employed to determine if a waste can be used in a construction material, according to the limits of Italian Ministerial Decree (Italian Ministerial Decree 186, 2006). In this case, RM could not be used since it exceeds the limits established for Se, Cr and Zn. CL present a low leaching of all heavy metals.

Table 4. RM and CL leachate composition (according to EN 12457-4) (mg/kg, dry basis)

Figure 2 and 3 shows the XRD patterns of RM and CL, respectively.

Figure 2. RM XRD pattern

Figure 3. CL XRD pattern

RM pattern showed a great broad peak in almost all 2θ range (4-70) which it is characteristic of an amorphous material. The amorphous content of RM, supplied by the DIFFRAC.EVA software, was 82.6 %. The main mineralogical phases were hematite, gibbsite and titanium nickel oxide. Besides, other phases were found such as iron aluminum oxides and titanium-manganese-vanadium iron oxides, whose reflection degrees coincided with the hematite.

The clay shows a behavior of a non-amorphous material (the amorphous content of CL supplied by the DIFFRAC.EVA software was 23.8 %). Some crystalline peaks of α-quartz mainly and muscovite and nontronite in less degree were detected. In addition, some organic compounds (methanol and oxadiazole) are also detected.

Thermogravimetric results of the red mud and the clay are showed in Figure 4.

Figure 4. Thermogravimetric analysis of RM and CL

Between ambient temperature and 473K, a mass loss due to the moisture is observed (2.6 %wt). Between 473K and 673K, there are three endothermic peaks for RM, due to the gibbsite dehydration to form boehmite and alumina (Liu et al, 2017). Weight loss of 2.52% between 673K and 1073K was because of the elimination of crystal water. Another weight loss of 0.28% was observed in the range 1173 – 1373K, due to the decomposition of some crystals. The sintering temperature was observed to be 1323K. A total mass loss of 13.1% was noted in raw RM during the thermal analysis.

When CL was heated from ambient temperature to 473K, the evaporation of physically-adsorbed and moisture water is produced (4 % of mass loss). Dehydration of nontronite, which happens between 333K and 433K (Frost et al, 2000) must be taken into account. From 473K to 673K, the weight remain essentially constant. In the range 673-1073K, a of 3% of mass loss occurred, probably due to the de-hydroxylation of muscovite (Yao et al, 2019) and nortronite (Frost et al, 2000) and the combustion of some organic compounds found in the CL (Leiva et al, 2016, Eliche-Quesada & Leite Costal, 2016). Above 1173K, there are no significant weight losses, although the sintering process of the clay begins at 1302K.

Figure 5 represents the XRD pattern of clay at 1373K (RM0-1100). As can be seen, it was not appreciable muscovite and some peaks of nontronite have disappeared. However, quartz remained in the clay. At 298K (Figure 3), quartz was α-quartz but at 1373K, DIFFRAC.EVA software showed quartz as quartz. A series of quartz phases transformation happens at high temperature (Jishi & Quiang, 2018): α-quartz transforms in β-quartz at 846K and around 1123K, β-quartz change to β-tridymite (this last did not appear in the XRD pattern of clay at 1373K). Amorphous content was determined by the DIFFRAC.EVA and the value was 29.2 %.

Figure 5. Clay XRD pattern at 1373K

Figure 6 shows the XRD pattern of raw materials (CL and RM) and RM80-900 and RM80-1100.

Figure 6. XRD patterns of RM and CL at 298K and RM80-900 and RM80-1100

Firstly, it can be observed that mixture RM80-900 shows similar XRD pattern than RM but with less amorphous content (73.1% calculated by DIFFRAC.EVA software). It is visualized peaks of hematite belongs to the red mud and quartz belongs to the clay remain at 1173K but peaks of gibbsite and titanium nickel oxides (from the red mud) and nontronite and muscovite (from the clay) have disappeared. RM80-1100 shows an amorphous content of 33.8 % (by means the DIFFRAC.EVA). Peaks of hematite and iron aluminium oxide were observed and silicon oxide was also appreciable. The main differences between samples calcined at 1173K and 1373K is the loss of amorphous phase (from 73.2 to 33.8 %) with the additional loss of peaks height at 1373K.

3.2. Physical and mechanical properties

As it can be seen in Figure 7, at the same RM percentage, the higher firing temperature, the higher the density. Even if RM and CL has a small mass loss between 900 and 1373K, as shown Figure 3, the increase of temperature causes two effects: 1) a higher sintering of RM and CL that produces a viscous amorphous phase which flows into the pores (Leiva et al, 2016) and 2) a shrinkage, as it can be observed in Figure 8. Both effects increase the density of the final material. During the sintering process, RM particles form a more compact and denser structure due to the decomposition of Na_2O (Kim et al, 2019, Mandal et al., 2017).

Figure 7. Density of samples after sintering

Figure 8. Samples after the heating cycles

Bulk densities in bricks are in between 1200–1400 kg·m^{-3}for burnt clay bricks (Alonso-Santurde et al, 2012). Density of bricks with high mechanical properties used to be in the range between 1700 and 2000 kg·m^{-3} (Eliche-Quesada et al, 2018). All tested dosages at 1373K show values within this interval or upper. All studied specimens showed densities higher than 1500 kg·m^{-3}, probably due to the high concentration of iron and titanium oxide in the RM, even at low sintering temperature (He et al, 2011).

Figure 9.Water absorption of samples after sintering

The higher the sintering temperature, the higher the shrinkage (Figure 8); however, the water absorption was just the opposite as Figure 9 shows, decreasing with the sintering temperature. Not all countries set a maximum water absorption content. According to China standards, water adsorption should be less than 20% (GB 5101, 2003). Only bricks produced at 1373K were suitable set the Chinese standards.

Figure 10. Compressive strength of samples after sintering

The compressive strength increased for all RM dosages when the sintering temperature increased (Figure 10) because sintering process increased the connection between the particles producing a brick with low high mechanical strength and low porosity. At 1173K, Rc decreased when RM content was increased, however, at 1373K, Rc enhanced with the increase of RM in the brick, due to the higher contents of Na_2O (Leiva et al, 2018)

ASTM C62-13 states that Rc > 10.3 MPa for normal weathering bricks and > 17.2 MPa for moderate weathering bricks (ASTM C62 – 13, 2013). In this case, only RM80-1100 could be used under both restrictions and RM50-1100 could be used in normal weathering. European standard for masonry units stablishes that Rc > 10 MPa for conventional bricks

(EN 771-1, 2016). They are meet for both RM content but only if 1373K is the firing temperature.

Rc is slightly lower than other previous studies using RM (He et al, 2011; Liu et al, 2017; Hegedüs et al, 2016) at similar temperatures, mainly due to the higher pressing molding (10-20 MPa) used in these studies.

3.3. Leaching results

Netherlands are leaders in recycling of by-product in construction materials and, minimizing deposits in landfills. By-products could be used in construction materials if in the NEN 7375 leachate (NEN 7375, 2005) from the final product, the contents of certain substances are below the limit values indicated in the Dutch Soil Quality Decree (SQD, 2007) for monolithic applications. SQD for molded materials sets the maximum amount per square meter for heavy metal in leachate. The results of the Dutch leaching test are shown in Table 5.

Table 5. Leaching results from NEN 7345 (mg/m^2)

As can be seen, Cd, Co, Hg, Ni, Hg, Se, Pb, Se, Sn, Sb, Sn and Th are not leached from the final products; Ba and Zn leaching values and Cu and Mo leaching values are under the 0,5% and 2% of the limit values respectively. As, Mo, V are quantitatively leached: the higher the RM dosage and the lower the sintering temperature, the higher the As, Mo, V concentrations.

As sintering temperature is increased, the leaching values diminished. It is due to the diminution of porosity produced in the bricks at higher temperatures, which means that the leaching solution cannot get to extract so many heavy metals. All the materials sintered at 1373K showed leaching values below the SQD limits, so they can be used in Netherlands without any restrictions. The only case that did not satisfy the SQD is the material RM80-900 for Vanadium.

Although Th is not a heavy metal, it is a radioisotope that has an important role in the radiological behavior and it did not leach, especially when it is heated to temperatures above 1073K (Hegedüs et al, 2016).

3.4 Natural radionuclide content

Radionuclides are present in by-products and natural building materials (European Commission, 1999). The 2013/59/EURATOM (European Commission, 2013) directive sets the requirements on the recycling of by-products into construction materials from its radiological impact. It sets a maximum gamma radiation exposure of 1.0 mSv/y for long-term exposure to natural radiation.

Activity concentration index (ACI) is used for the evaluation of the fulfillment of a building material. This index can be calculated as a function of the activity concentrations of Th-232, Ra-226, and K-40 (the major natural radionuclides) as shown in equation 1:

$$ACI=C_{Th\text{-}232}/200 + C_{K\text{-}40}/3000 + C_{Ra\text{-}226}/300 \qquad \text{(eq. 1)}$$

where $C_{Th\text{-}232}$, $C_{K\text{-}40}$ and $C_{Ra\text{-}226}$, are the activity concentrations of Th-232, K-40 and Ra-226 in Bq/kg. To fulfill the requirement of 1.0 mSv/y for the annual dose, a construction material must present ACI < 1.0 (Table 6).

Compared to other bauxite residues, this RM exhibits similar concentrations of Th-232 (219–392 Bq/kg), Ra-226 (225–568 Bq/kg) and K-40 (4.9–101 Bq/kg) (Croymans et al, 2017; Somlai et al, 2008, Nuccetelli et al, 2017). The type of bauxite utilized to produce the aluminium products is the primary factor governing the radiological content of Th-232 and Ra-226 in RM (Von Philipsborn & Kuhnast, 1992).

CL presents a high K-40 activity concentration than RM, but it is within the usual range of the clay (518–843 Bq/kg), similarly than Th-232 (35-75 Bq/kg) and Ra-226 (30-52 Bq/kg).

Table 6. Major radionuclides activity concentrations (Bq/kg) and activity concentration indexes

As can be observed, only the composition with the lowest percentage of RM (RM50-1100) satisfies the criterion of ACI <1 and very little, while the compositions with 80% red mud present ACI> 1, independently of the sintering temperature. These values are higher than other bricks with use other by-products at similar temperatures and dosages (coal fly ashes (Leiva et al, 2018), co-combustion fly ashes (Leiva et al, 2016) or manganese by-products (Kovács et al, 2017)).

ACI is undoubtedly a tool that is widely used to assess the radiological behavior of building materials. But, it does not consider the real density and thickness of building products, otherwise it consider a specific density (2350 kg/m^{-3}) and thickness (0.2 m) (Nuccetelli et al, 2015). Therefore, equation 1 should be modified with two weighting factors related to density and thickness (CEPMC, 2011) according to eq. 2:

$$ACI_d = (C_{Ra-226}/300 + C_{Th-232}/200 + C_{K-40}/3000) \cdot \rho \cdot d/470 \qquad \text{(eq. 2)}$$

where ρ is the density of the considered material (kg/m^3), d is the wall thickness (m) and 470 is the weight per unit area according to the model of European radiological protection principles (European Commission, 1999) for the concrete (ρ = 2350 kg/m^3 and d = 0.2 m). Table 6 shows the ACI_d for the different compositions using the real density of the bricks (Figure 3) and assuming a thickness of 0.05 m, since this is the largest thickness that is usually found in bricks.

In this case, ACI_d is lower than ACI because the bricks have a lower density than the concrete and the thickness is also, although this decrease in RM80-1100 is less pronounced, due to its higher density due to its advanced sintering process. If $ACI_d<1$ is used as limit value, all the different compositions at different present values lower than 0.5, which would involve receiving smaller doses of 0.3 mSv/y.

5. Conclusions

- At firing temperature higher than sintering temperature, higher density, lower water absorption and higher compression strength are observed when the amount of red mud is increased, due to the increase in sintering process.

- At firing temperatures lower than red mud`sfusion , the higher the red mud addition, the lower the density and compressive strength, but at higher temperatures the addition of RM increases both parameters.

- From heavy metals leaching point of view, the bricks could be used as construction materials in Netherlands but not in Italy. In the opinion of the authors, it would be necessary to homogenize the regulations and employing environmental tests similar to what can happen in reality.

- The radiological behavior should be studied in construction materials with red mud, due to the enhanced content of natural radionuclides. Taking into account the ACI the material, they are in the limit to be allowed as construction material; however, if the density correction is included, it fits below the limit values.

6. References

Alonso-Santurde, R., Coz, A., Viguri, J.R., Andrés, A, 2012. Recycling of foundry by-products in the ceramic industry: green and core sand in clay bricks. Constr. Build. Mater. 27, 97-106. https://doi.org/10.1016/j.conbuildmat.2011.08.022.

ASTM C62-13a. Standard Specification for Building Brick (Solid Masonry Units Made From Clay or Shale. 2013. ASTM International, West Conshohocken, PA. https://doi.org/10.1520/C0062-13.

B192. Bekendtgørelse nr. 192 af 2 ‘‘Bekendtgørelse om undtagelsesregler fralov om brug m.v. af radioaktive stoffer”, The National Institute of Radiation Hygiene, Herlev, Denmark; 2002

CEPMC. Position paper. European Commission Services considerations with regard to natural radiation sources Basic Safety Standards Directive. 2011. TG DS 11-06. Council of European Producers of Materials for Construction. Brussels.

Croymans, T., Schroeyers, W., Krivenko, P., Kovalchu, O., Pasko, A., Hult, M., Marissens, G., Lutter, G., Schreurs, S., 2017. Radiological characterization and evaluation of high volume bauxite residue alkali activated concretes. J. Environ. Radioactiv. 168, 21-29. https://doi.org/10.1016/j.jenvrad.2016.08.013.

DPV. 2003. Decreto 34 del País Vasco por el que se regula la valorización y posterior utilización de escorias procedentes de la fabricación de acero en hornos de arco eléctrico, en el ámbito de la Comunidad Autónoma del País Vasco.

Eliche-Quesada, D., Leite-Costa, J., 2016. Use of bottom ash from olive pomace combustion in the production of eco-friendly fired clay brick. Waste Manage. 48, 323–333. https://doi.org/10.1016/j.wasman.2015.11.042.

Eliche-Quesada, D., Sandalio-Pérez, J.A., Martínez-Martínez, S., Pérez-Villarejo, L., Sánchez-Soto, P.J., 2018. Investigation of use of coal fly ash in eco-friendly construction materials: fired clay bricks and silica-calcareous non fired bricks. Ceram. Int. 44(4), 4400-4412. https://doi.org/10.1016/j.ceramint.2017.12.039.

EN 12457-4. 2002. Characterization of waste: Leaching. Compliance test for leaching of granular waste material and sludges. Part 2: One stage batch test at a liquid to solid ratio of 10 l/kg for materials with particle size below 10 mm (without or with size reduction).

EN 771-1. 2016. Specification for masonry units-Part 1: clay masonry units.

EN 772-1. 2016. Methods of test for masonry units - Part 1: Determination of compressive strength.

EN 772-13. 2013. Methods for mansory units Part 13. Determination of net and gross dry density of mansory units (except for natural Stone).

EN 772-21. 2011. Methods for mansory units Part 21. Determination of water absorption of clay and calcium silicate mansory units by cold water absorption.

European Commission. Council directive No 305/2011 of the European Parliament and of the Council of 9 March 2011 laying down harmonised conditions for the marketing of construction products and repealing Council Directive 89/106/EEC. Brussels; 2011.

European Commission. 1999. Radiation Protection 112. Radiological Protection Principles Concerning the Natural Radioactivity of Building Materials. Luxembourg, ISBN: 92-828-8376-0. (1999).

European Commission. 2013. Council directive 2013/59/EURATOM of 5 December 2013 laying down basic safety standards for protection against the dangers arising from exposure to ionising radiation. Brussels.

Frost, R.L., Ruan, H., Kloprogge, J.T., Gates, W.P. 2000. Dehydration and dehydroxylation of nontronites and ferruginous smectite. Thermochim. Acta. 346 (1–2), 63-72. https://doi.org/10.1016/S0040-6031(99)00366-4.

GB 5101. 2003. Fired Common Bricks. General Administration of Quality Supervision Inspection and Quarantine of China China Standard Press, Beijing. http://www.samr.gov.cn/.

He H, Yue Q, Su Y, Gao B, Gao Y, Wang J, Yu H. 2011. Preparation and mechanism of the sintered bricks produced from Yellow River silt and red mud. J. Hazard. Mater. 53-61. https://doi.org/10.1016/j.jhazmat.2011.11.095.

Hegedüs, M., Sas, Z., Tóth-Bodrogi, E., Szántó, T., Somlai, J., Kovács, T., 2016. Radiological characterization of clay mixed red mud in particular as regards its leaching features. J. Environ. Radioactiv. 162-163 (10), 1-7. https://doi.org/10.1016/j.jenvrad.2016.05.002.

Italian Ministerial Decree 186. Identification of non-hazardous waste subjected to simplified recovery procedures pursuant to articles 31 and 33 of the legislative decree 05/02/1997. Gazzetta Ufficiale 2006 n. 115 (2006)

Jishi, G., Quiang, S., 2018. Effects of high temperature treatment on physical-thermal properties of clay. Thermochim. Acta. 666, 148-155. https://doi.org/10.1016/j.tca.2018.06.018.

Kim, Y., Lee, Y, Kim, M., Park, H.; 2019. Preparation of high porosity bricks by utilizing red mud and mine tailing. J. Clean. Prod. 207, 490-497. https://doi.org/10.1016/j.jclepro.2018.10.044.

Kovács, T., Shahrokhi, A., Sas, Z., Vigh T., János, S., 2017. Radon exhalation study of manganese clay residue and usability in brick production. J. Environ. Radioactiv. 168, 15-20. https://doi.org/10.1016/j.jenvrad.2016.07.014.

Leiva, C., Arenas, C., Alonso-Fariñas, B., Vilches, L.F., Peceño, B., Rodriguez-Galán, M., Baena, F., 2016. Characteristics of fired bricks with co-combustion fly ashes. J. Build. Eng. 5 (1), 114-118. https://doi.org/10.1016/j.jobe.2015.12.001.

Leiva, C., Rodriguez-Galán, M., Arenas, C., Alonso-Fariñas, B., Peceño, B. 2018. A mechanical, leaching and radiological assessment of fired bricks with a high content of fly ash. Ceram. Int. 44(11), 13313-13319. https://doi.org/10.1016/j.ceramint.2018.04.162.

Luo, L., Li, K., Weng, F., Liu, Ca, Yang, S. 2020. Preparation, characteristics and mechanisms of the composite sintered bricks produced from shale, sewage sludge, coal gangue powder and iron ore tailings. Constr. Build. Mater. 30 117250. DOI: 10.1016/j.conbuildmat.2019.117250.

Liu, S., Guan, X., Zhang, S., Dou, Z., Feng, C., Zhang, H., Luo, S., 2017. Sintered bayer red mud based ceramic bricks: Microstructure evolution and alkalis immobilization mechanism. Ceram. Int. 43 (15), 13004-13008. doi.org/10.1016/j.ceramint.2017.07.036.

Mahinroosta, M., Karimi, Z., Allahverdi, A. 2020. Recycling of Red Mud for Value-Added Applications: A Comprehensive Review. Encyclopedia of Renewable and Sustainable Materials. 2, 561-582. https://doi.org/10.1016/B978-0-12-803581-8.11474-2

Man, K., Zhu, Q., Li, L., Liu, C., Xing, Z., 2017. Preparation and performance of ceramic filter material by recovered silicon dioxide as major leached component from red mud. Ceram. Int. 43 (10), 7565-7572. https://doi.org/10.1016/j.ceramint.2017.03.048.

Mandal, A.K.; Verma, H.R.; Sinha, O.P.; 2017. Utilization of aluminum plant's waste for production of insulation bricks. J. Clean. Prod. 162, 949-957. https://doi.org/10.1016/j.jclepro.2017.06.080.

Maza-Ignacio, O.T., Jiménez-Quero, V.G., Guerrero-Paz, J., Montes-García, P. 2020. Recycling untreated sugarcane bagasse ash and industrial wastes for the preparation of resistant, lightweight and ecological fired bricks. Constr. Build. Mater. 23420, 117314. https://doi.org/10.1016/j.conbuildmat.2019.117314

NEN 7375. Leaching characteristics - Determination of the leaching of inorganic components from moulded or monolitic materials with a diffusion test - Solid earthy and stony materials (2005).

Nuccetelli, C., Pontikes, Y.F., Rosabianca, L.T., 2015. New perspectives and issues arising from the introduction of (NORM) residues in building materials: A critical assessment on the radiological behavior. Constr. Build. Mater. 82, 323-331. https://doi.org/10.1016/j.conbuildmat.2015.01.069.

Nuccetelli, C., Risica, S., Onisei, S., Leonardi, F., Trevisi, R., 2017. Natural radioactivity in building materials in the European Union: a database of activity concentrations and radon exhalations (No. 17/36), Rapporti ISTISAN. 2017, 70 p.

Oprčkal, P., Mladenovič, A., Zupančič, N., Ščančar, J., Milačič, R., Zalar-Serjun V. 2020. Remediation of contaminated soil by red mud and paper ash. J. Clean. Prod. 25620, 120440. https://doi.org/10.1016/j.jclepro.2020.120440

OVS. 1996. Order on Valorization of Slags of Catalunya of 15 February 1996. Generalitat de Catalunya DO 2181.

Pérez-Villarejo, L., Corpas-Iglesias, F.A., Martínez-Martínez, S., Artiaga, R., Pascual-Cosp, J. 2012. Manufacturing new ceramic materials from clay and red mud derived from the aluminium industry. Constr. Build. Mater. 35, 656-665. https://doi.org/10.1016/j.conbuildmat.2012.04.133

Rehman, M.U, Ahmad, M., Rashid, K. 2020. Influence of fluxing oxides from waste on the production and physico-mechanical properties of fired clay brick: A review. J. Build. Eng., 27, 100965 https://doi.org/10.1016/j.jobe.2019.100965

SI 5098, Content of natural radioactive elements in building products, Standard of Israel No. 5098, The Standards Institution of Israel, Tel-Aviv, Israel; 2007

SQD. Soil Quality Decree Dutch Ministry of Housing Spatial Planning and the Environment. (Besluitbodemkwaliteit). (2007)

Somlai, J., Jobbágy, V. Kovács, J.; Tarján, S., Kovács, T., 2008. Radiological aspects of the usability of red mud as building material additive. J. Hazard. Mater. 150 (3), 541-545. https://doi.org/10.1016/j.conbuildmat.2017.05.167.

Von Philipsborn, H., Kuhnast, E., 1992. Gamma spectrometric characterisation of industrially used African and Australian bauxites and their red mud tailings. Radiat. Prot. Dosim. 45 (1–4 Suppl.), 741-743. https://doi.org/10.1093/rpd/45.1-4.741.

Wang, W., Sun, K., Haitao Liu H. 2020. Effects of different aluminum sources on morphologies and properties of ceramic floor tiles from red mud. Constr. Build. Mater. 24130, 118119. https://doi.org/10.1016/j.conbuildmat.2020.118119

Yao, G., Zang, H., Wang, J., Wu, P., Qiu, J., Lyu, X. 2019. Effect of mechanical activation on the pozzolanic activity of muscovite. Clays Clay Miner. 67 209. https://doi.org/10.1007/s42860-019-00019-y

Zhang, L. 2013. Production of bricks from waste materials – A review. Constr. Build. Mater. 47, 643-655. https://doi.org/10.1016/j.conbuildmat.2013.05.043

Zhang, J., Li, P., Liang, M., Jiang, H., Yao, Z., Zhang, X., Yu S. 2020. Utilization of red mud as an alternative mineral filler in asphalt mastics to replace natural limestone powder. Constr. Build. Mater. 237, 117821. https://doi.org/10.1016/j.conbuildmat.2019.117821

Tables from 1 to 6

Table 1. Compositions of bricks (%wt)

	CL	RM	H_2O		CL	RM	H_2O
RM0-900	32	0	68	**RM0-1100**	32	0	68
RM50-900	16	16	68	**RM50-1100**	20	20	60
RM80-900	9	36	55	**RM80-1100**	9	36	55

Table 2. Clay and red mud chemical characterization (%wt)

Parameter	RM	CL
SiO_2	4.87	75.66
Al_2O_3	18.08	11.25
Fe_2O_3	50.89	3.06
CaO	1.13	1.47
K_2O	0.07	3.55
MgO	0.07	1.48
Na_2O	3.45	0.11
TiO_2	9.33	-
P_2O_5	0.45	-
MnO_2	0.07	-
Loss on ignition	10.26	3.37
Moisture (%wt)	-	3.53
Specific gravity(g/cm^3)	2.85	2.45

Table 3. Minor chemical components (ppm) of RM

As	Ba	Br	Ni	Cr	Cu	Ga	Th	Hf	I	La	Mn	Mo
63.9	193.7	4.0	17.3	1818	74.9	73.4	121.8	20.2	14.7	112.6	276.4	12.3
Sb	**Nd**	**Se**	**Sr**	**Sn**	**Ta**	**U**	**V**	**W**	**Y**	**Nb**	**Zn**	**Pb**
5.6	84.1	2.9	93.9	9.3	7.0	13.0	1169	48.2	115.8	161.2	46.0	62.0

Table 4. RM and CL leachate composition (according to EN 12457-4) (mg/kg, dry basis)

	Cd	Ba	Co	Cu	Cr	Hg	Ni	Mo	Pb	Se	Sb	V	As	Zn
RM	<0.02	0.09	0.02	0.14	25.75	<0.01	<0.05	0.27	<0.05	0.36	0.31	1.33	<0.02	1.11
CL	<0.02	<0.01	<0.01	<0.01	<0.01	<0.01	0.33	<0.01	<0.05	<0.02	0.11	<0.02	0.07	0.32
IMD 186	0.05	10	2.5	0.5	0.5	0.01	0.1	-	0.5	0.1	-	2.5	0.5	0.03

Table 5. Leaching results from NEN 7345 (mg/m^2)

	DSQ Limits	RM0-900	RM0-1100	RM50-900	RM50-1100	RM80-900	RM80-1100
As	260	0.73	0.15	4.49	4.54	13.59	1.43
Ba	1500	0.19	0.42	0.10	0.15	<0.07	<0.07
Cd	3.8	<0.07	<0.07	<0.07	<0.07	<0.07	<0.07
Co	60	<0.15	<0.15	<0.15	<0.15	<0.15	<0.15
Cr	120	<0.15	<0.15	13.08	0.18	78.03	0.32
Cu	98	1.15	<0.15	<0.15	<0.15	<0.15	<0.15
Hg	1.4	<1.4	<1.4	<1.4	<1.4	<1.4	<1.4
Mo	144	0.07	0.07	1.15	0.57	2.51	0.70
Ni	81	<0.07	<0.07	<0.07	<0.07	<0.07	<0.07
Pb	400	<0.37	<0.37	<0.37	<0.37	<0.37	<0.37
Sb	8.7	<0.37	<0.37	<0.37	<0.37	<0.37	<0.37
Se	4.8	<0.37	<0.37	<0.37	<0.37	<0.37	<0.37
Sn	50	<0.15	<0.15	<0.15	<0.15	<0.15	<0.15
Th	-	<0.37	<0.37	<0.37	<0.37	<0.37	<0.37
V	320	5.29	0.76	190.70	34.35	337.85	51.19
Zn	800	1.68	<0.18	0.25	0.22	0.57	0.44

Table 6. Major radionuclides activity concentrations (Bq/kg) and activity concentration indexes

	Materials	RM	CL	RM0-1100	RM50-1100	RM80-900	RM80-1100
Radionuclides	K-40	98	650	618	355	204	198
	Ra-226	235	35	11	41	78	59
	Th-234	249	37	33	129	196	186
Indexes	ACI	-	-	0.41	0.90	1.31	1.19
	ACI_d	-	-	0.08	0.15	0.21	0.27

Figure 1

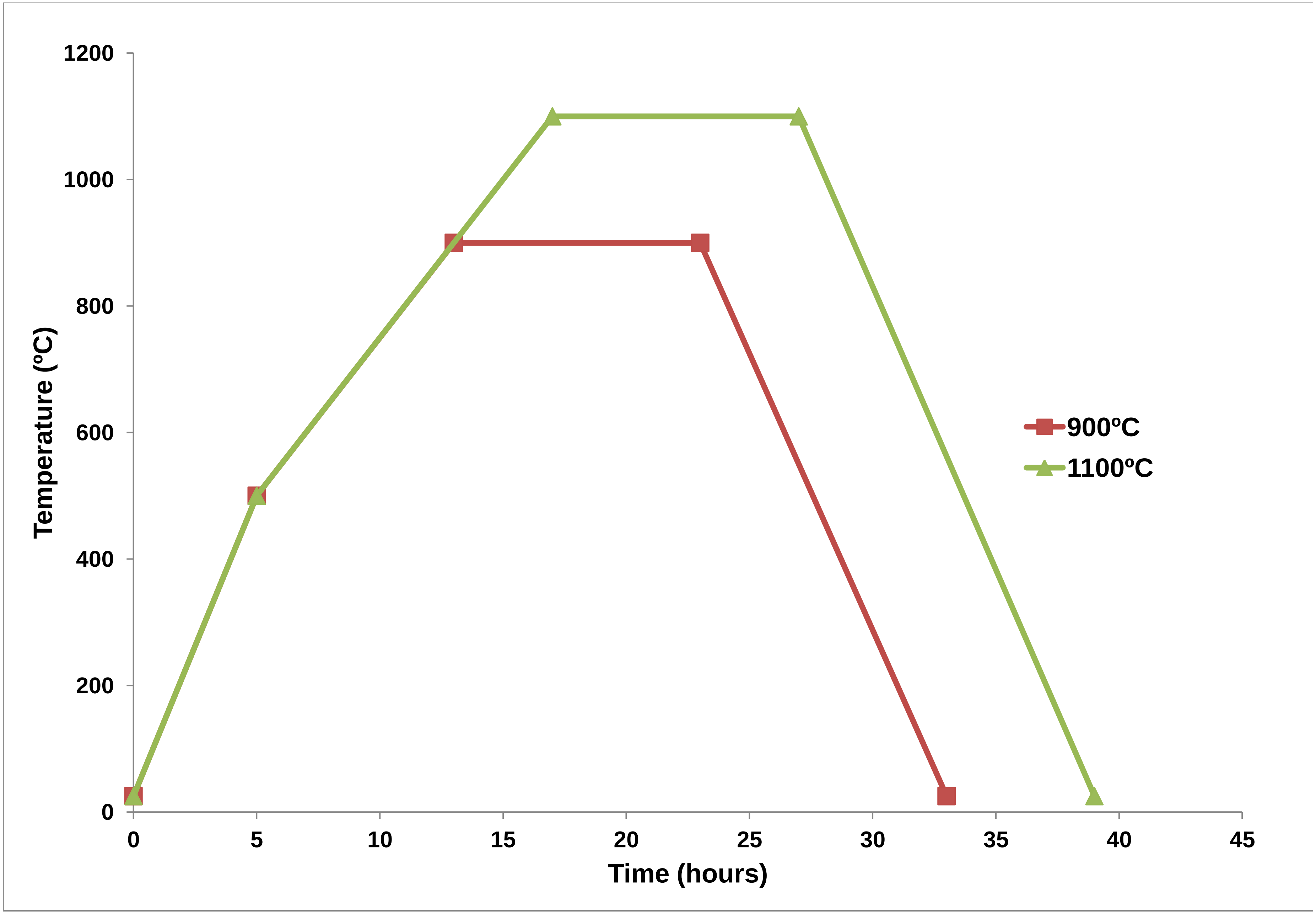
1200
1000
800
600
400
200
0
0
5
10
15
20
25
30
35
40
45
Temperature (ºC)
Time (hours)
900ºC
1100ºC

Figure 2

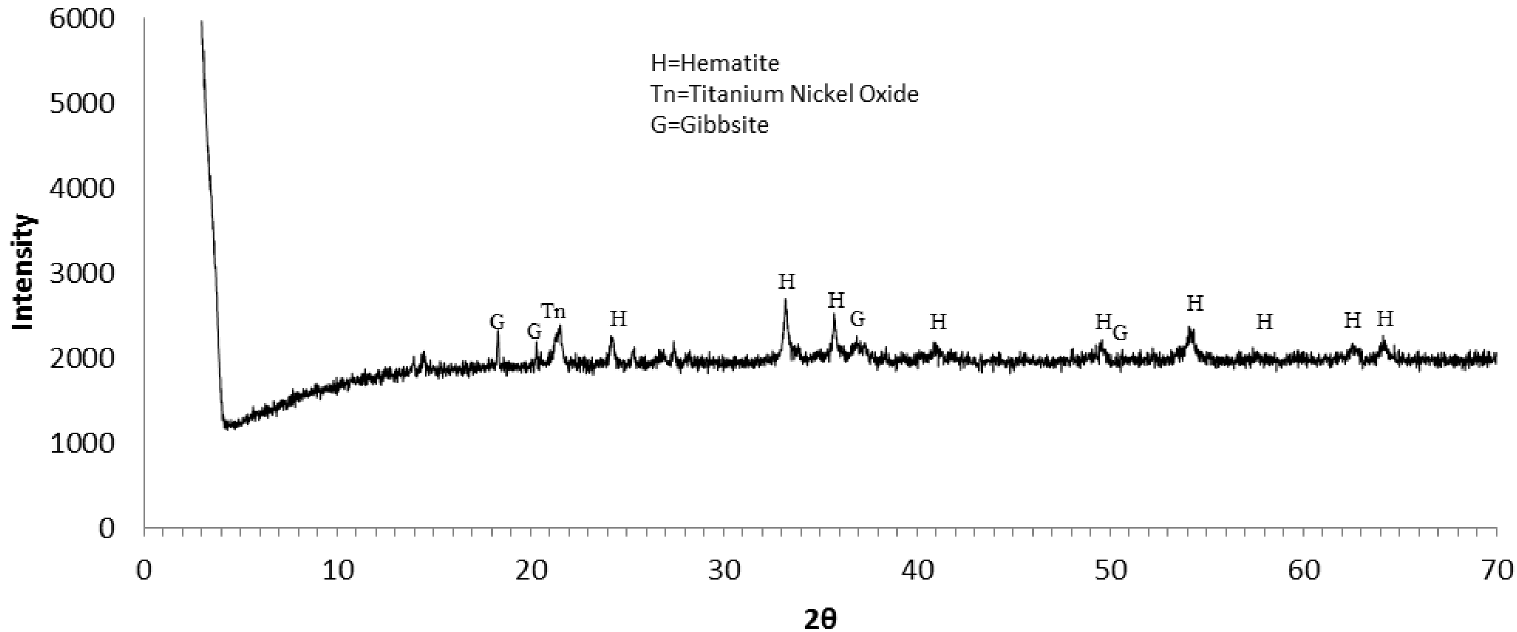
H=Hematite
Tn=Titanium Nickel Oxide
G=Gibbsite
Intensity
6000
5000
4000
3000
2000
1000
0
0
10
20
30
40
50
60
70
2θ
G
G
Tn
H
H
H
G
H
H
G
H
H
H
H

Figure 3

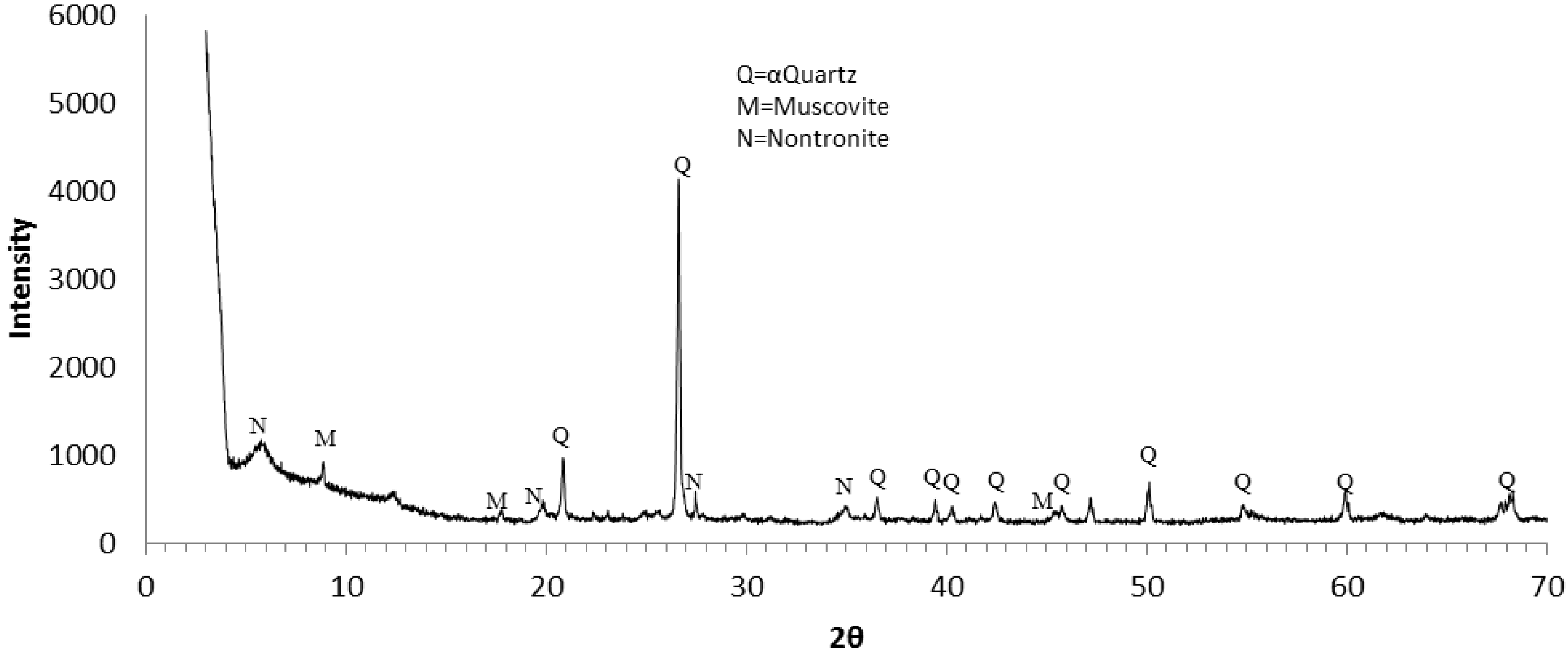

Q=αQuartz
M=Muscovite
N=Nontronite
Intensity
6000
5000
4000
3000
2000
1000
0
0
10
20
30
40
50
60
70
2θ
Q
N
M
M
N
Q
N
N
Q
Q
Q
Q
M
Q
Q
Q
Q
Q

Figure 4

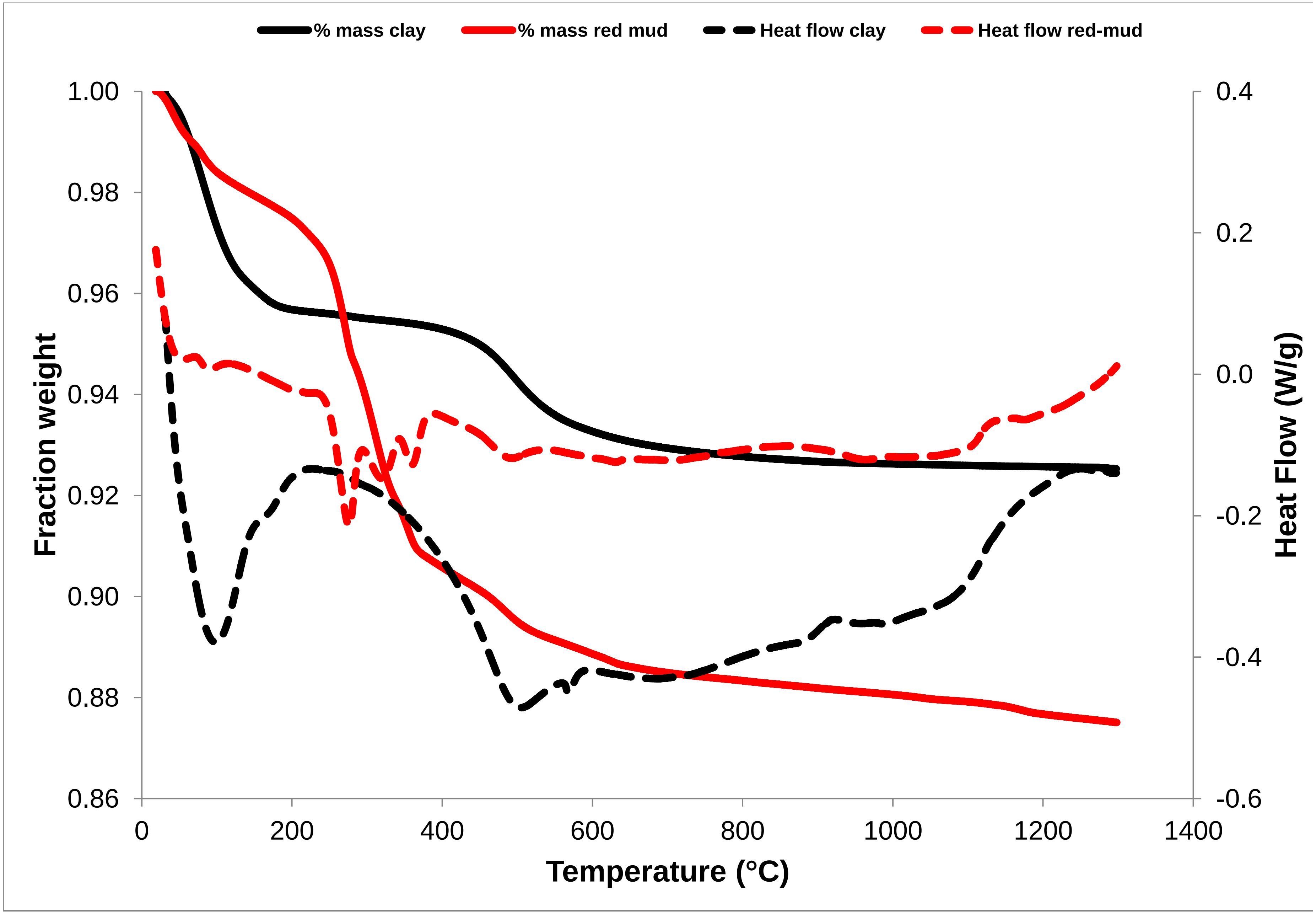

% mass clay
% mass red mud
Heat flow clay
Heat flow red-mud
1.00
0.98
0.96
0.94
0.92
0.90
0.88
0.86
Fraction weight
0.4
0.2
0.0
-0.2
-0.4
-0.6
Heat Flow (W/g)
0
200
400
600
800
1000
1200
1400
Temperature (°C)

Figure 5

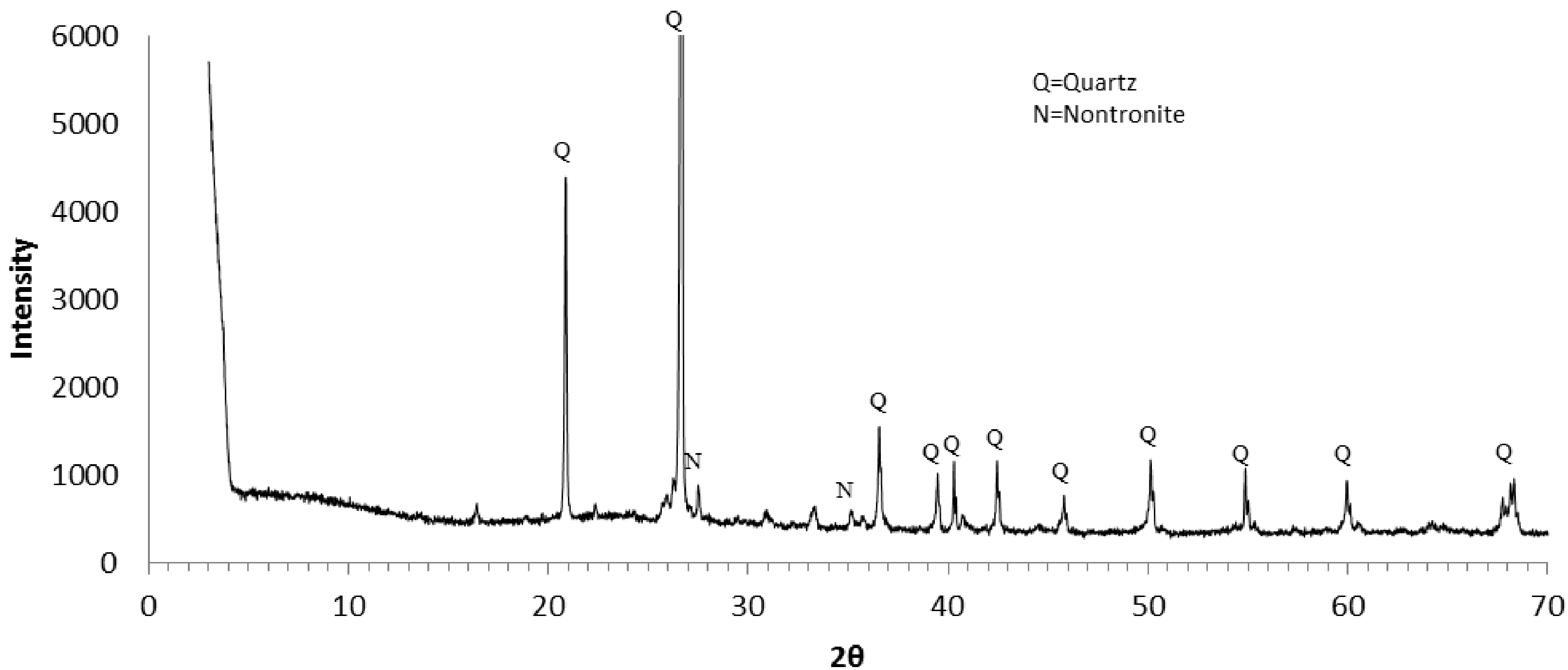

Q=Quartz
N=Nontronite
Intensity
2θ
6000
5000
4000
3000
2000
1000
0
0
10
20
30
40
50
60
70
Q
Q
N
N
Q
Q
Q
Q
Q
Q
Q
Q
Q

Figure 6

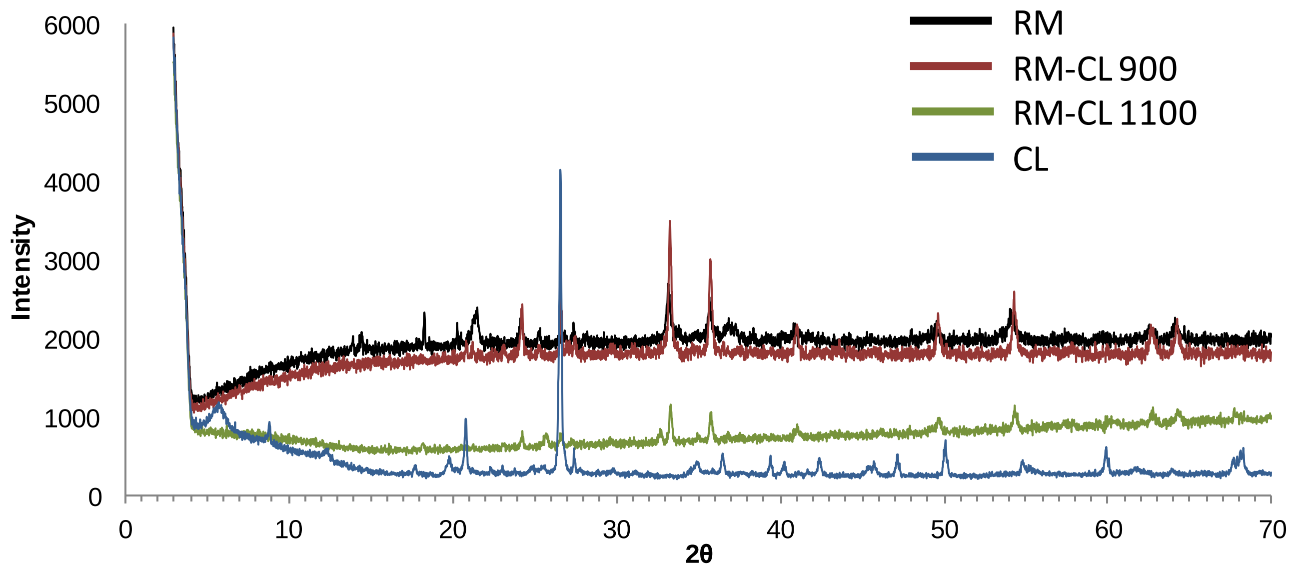

RM
RM-CL 900
RM-CL 1100
CL
Intensity
6000
5000
4000
3000
2000
1000
0
0
10
20
30
40
50
60
70
2θ

Figure 7

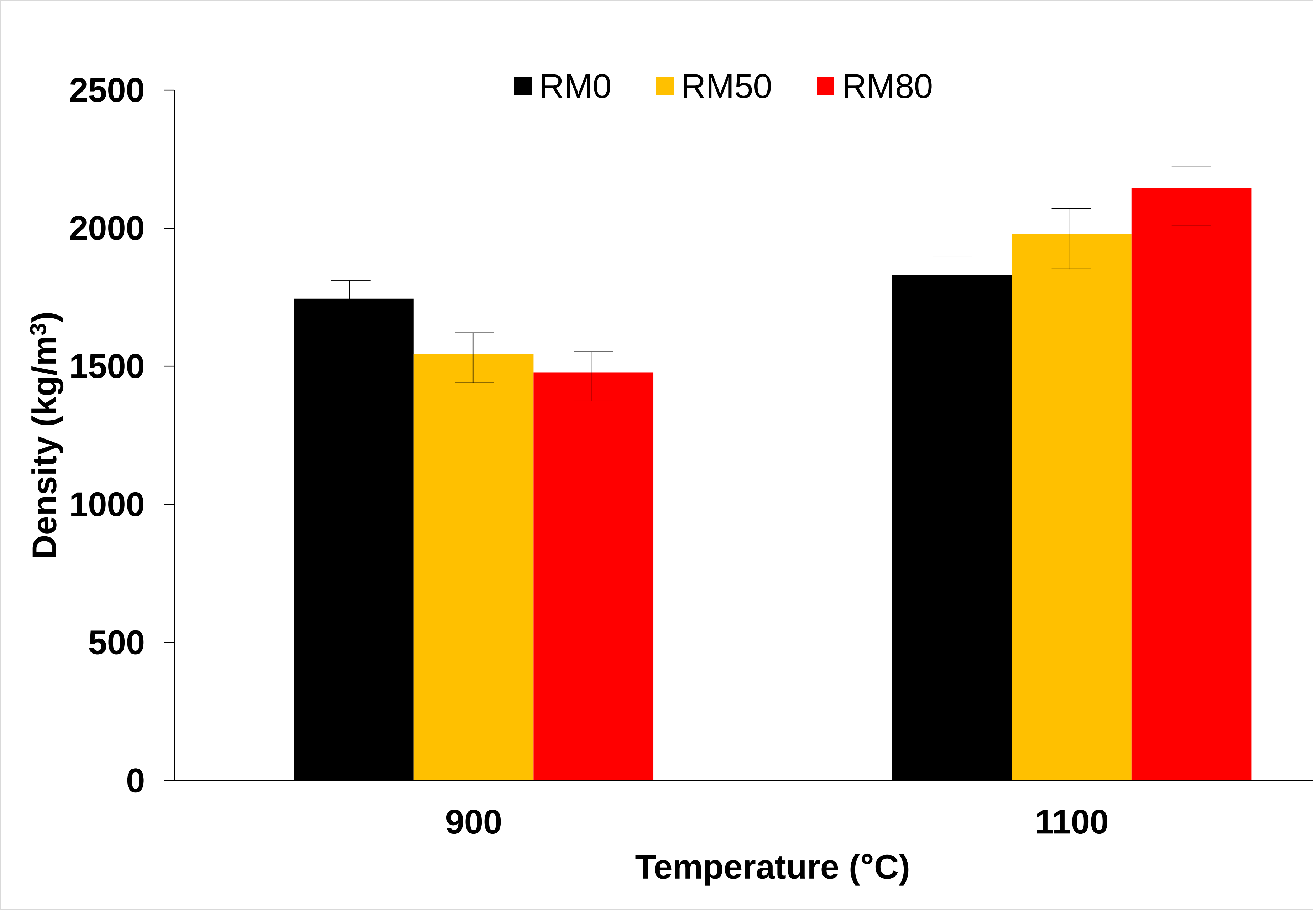

RM0
RM50
RM80
2500
2000
1500
1000
500
0
Density (kg/m³)
900
1100
Temperature (°C)

Figure 8

Figure 9

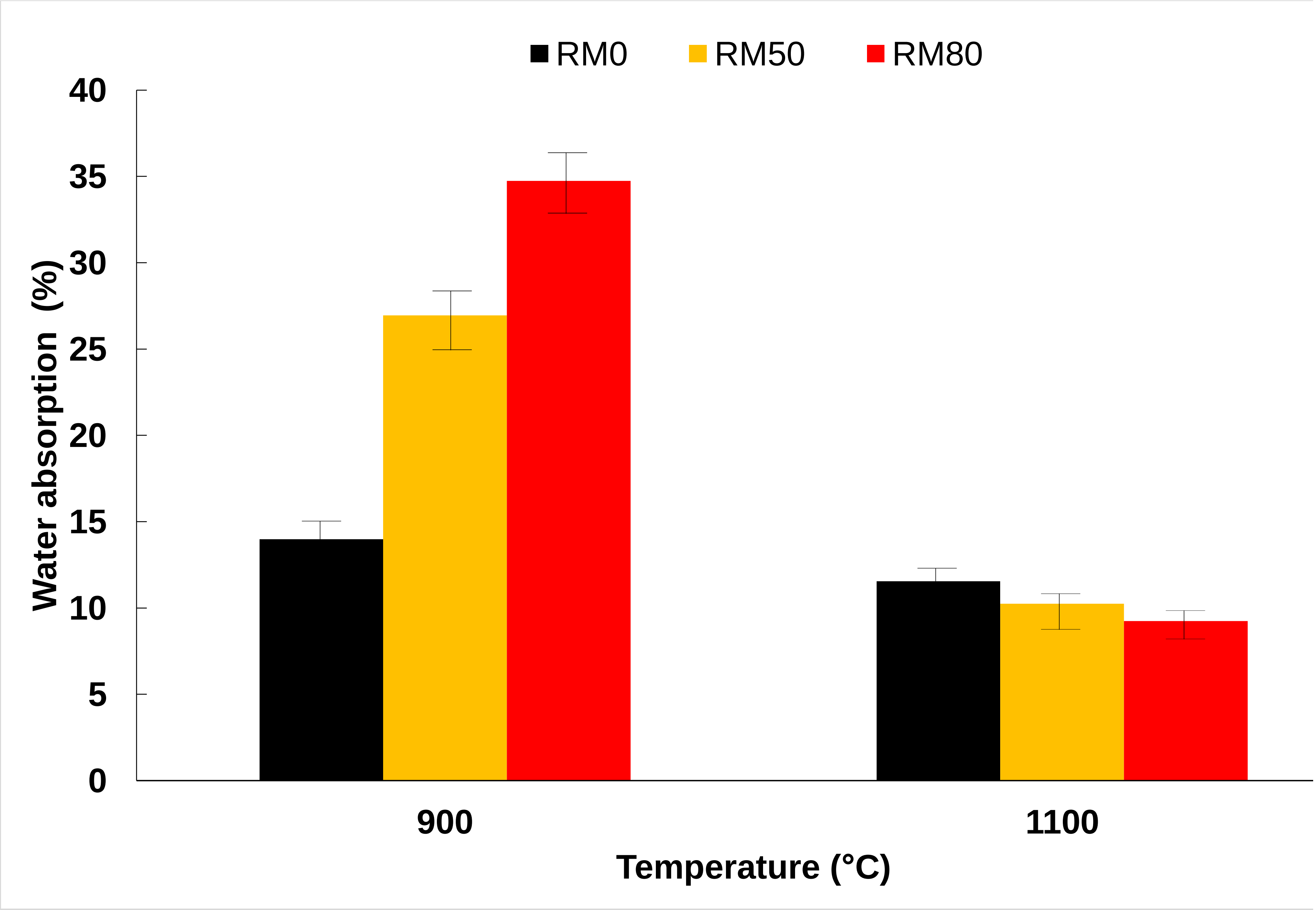

RM0
RM50
RM80
Water absorption (%)
40
35
30
25
20
15
10
5
0
900
1100
Temperature (°C)

Figure 10

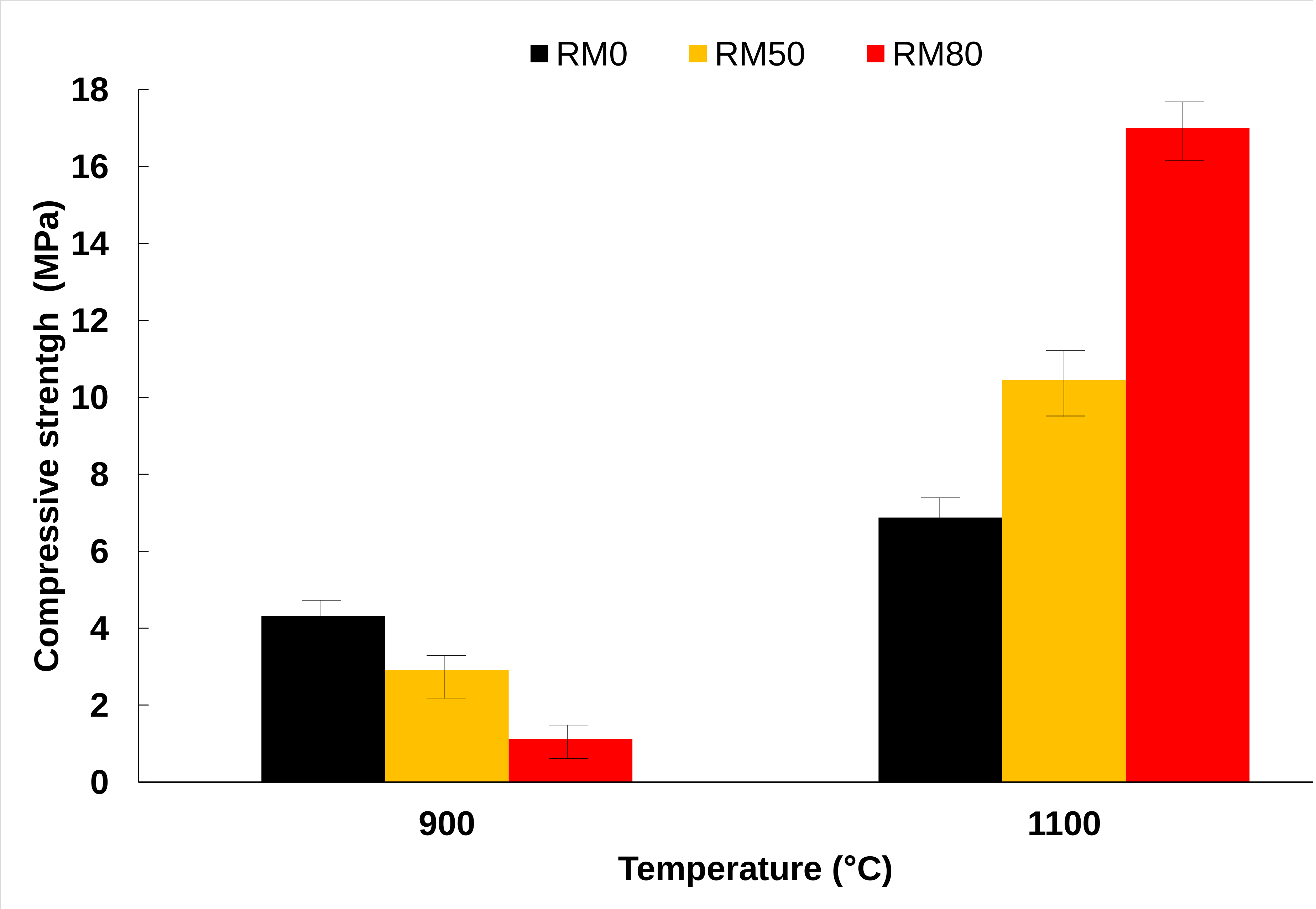
RM0
RM50
RM80
Compressive strentgh (MPa)
0
2
4
6
8
10
12
14
16
18
900
1100
Temperature (°C)